Electronic Supplementary Material (ESI) for Physical Chemistry Chemical Physics.

Supporting Information

In Situ Studies of the Cathodic Stability of Single-Crystalline IrO_2(110) Ultrathin Films Supported on RuO_2(110)/Ru(0001) in an Acidic Environment

Tim Weber[a,b], Marcel J. S. Abb[a,b], Jonas Evertsson[a,c], Martina Sandroni[d], Jakub Drnec[d], Vedran Vonk[c], Andreas Stierle[c,e], Edvin Lundgren[f], Herbert Over[a,b]*

a) *Institute of Physical Chemistry, Justus Liebig University, Heinrich-Buff-Ring 17, 35392 Giessen, Germany*
b) *Center for Materials Research, Justus Liebig University, Heinrich-Buff-Ring 16, 35392 Giessen, Germany*
c) *Deutsches Elektronen-Synchrotron (DESY), D-22607 Hamburg, Germany*
d) *Experimental Division, European Synchrotron Radiation Facility (ESRF), 71 Avenue des Martyrs, 38000 Grenoble, France*
e) *Fachbereich Physik University Hamburg, Jungiusstrasse 9, D-20355 Hamburg, Germany*
f) *Synchrotron Radiation Research, Lund University, Box 118, S-22100 Lund, Sweden*

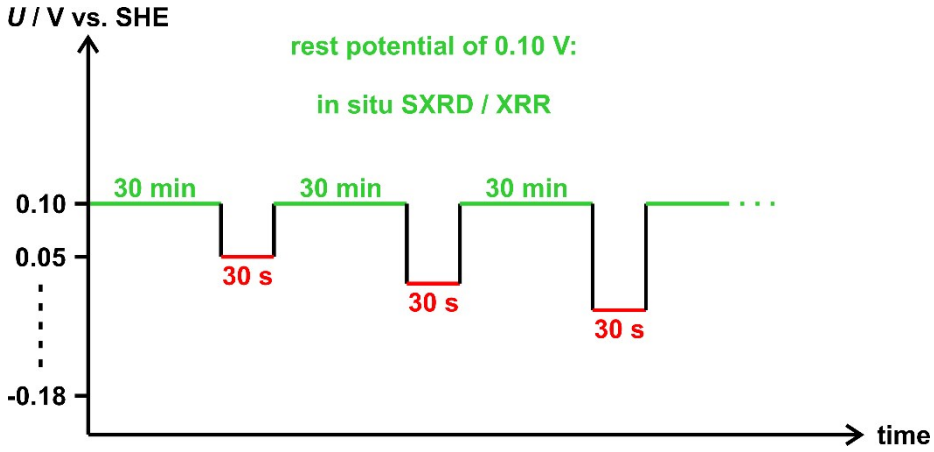

Figure S1: Schematic representation of the pulse-rest protocol applied within the in situ experiments.

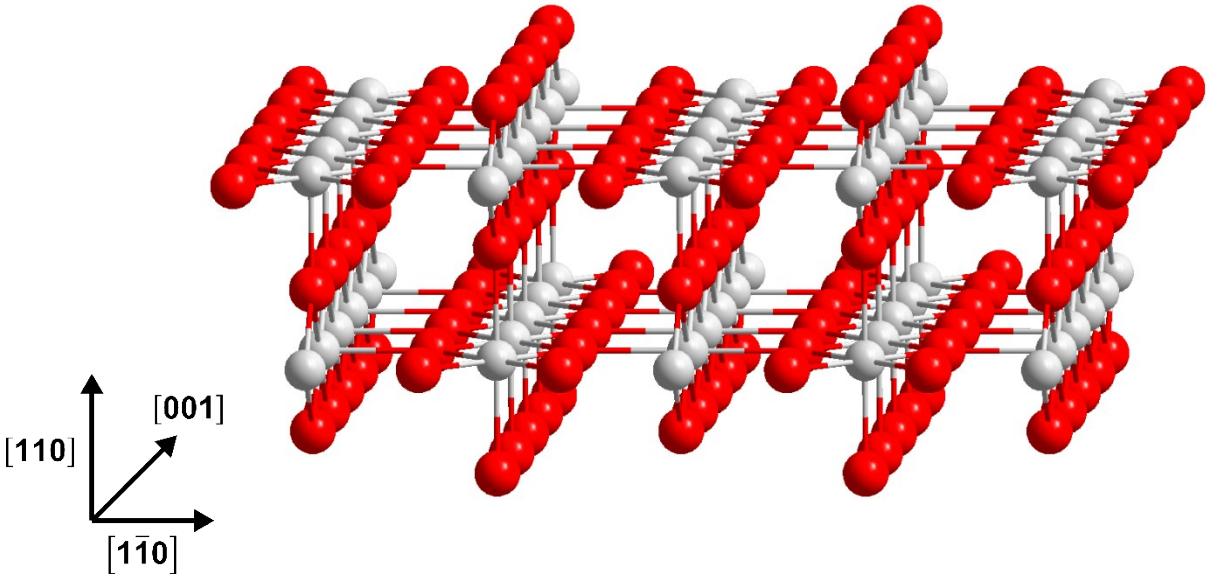

Figure S2: Ball and stick model of the $IrO_2(110)$ surface. The grey and red spheres represent the iridium and oxygen atoms, respectively. The coordinate system gives the relevant crystallographic directions.

Figure S2 shows the rutile $IrO_2(110)$ surface with the relevant crystallographic directions given in the coordinate system. The *h* and *l* directions in reciprocal space correspond to the crystallographic $[1\bar{1}0]$ and $[110]$ directions, respectively. For this reason, *h*- and *l*-scans allow to derive the lattice parameters and domain sizes in each direction from the peak positions and FWHM values, respectively, and to monitor possible alterations of them upon cathodic polarization. The *k* direction in reciprocal space corresponds to the crystallographic $[001]$ direction. However, in the present study *k*-scans were not conducted.

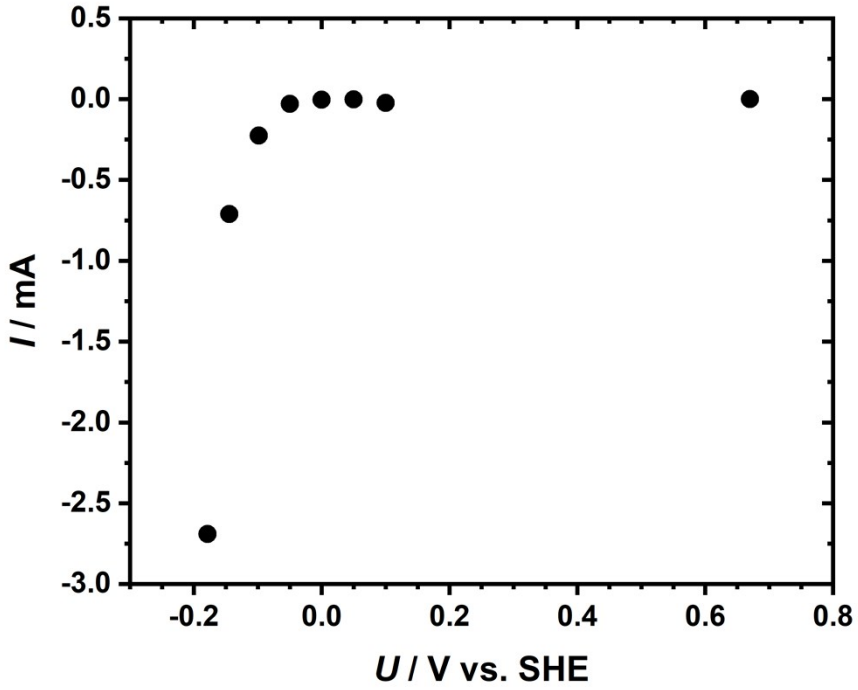

Figure S3: Current-potential diagram of the $IrO_2(110)$-$RuO_2(110)$/Ru(0001) model electrode within the in situ experiments.

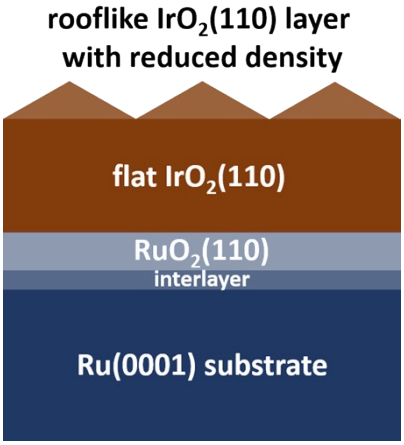

Figure S4: Schematic representation of the four-layer model employed for the simulation of the XRR data of the $IrO_2(110)$-$RuO_2(110)$/Ru(0001) model electrode (modified and reprinted with permission from Weber et al.[1] Copyright 2019 American Chemical Society).

Table S1: Fitting parameters of the XRR data of the $IrO_2(110)$-$RuO_2(110)$/Ru(0001) model electrode

at open-circuit potential (OCP) and –0.14 V vs. SHE. The X-ray beam with an energy of 21.5 keV (λ = 57.67 pm) was modelled with a Gaussian shape, the beam with was set 200 µm. The values highlighted in orange or blue either hit the default limit or were kept constant, respectively. *d* denotes the thickness of a specific layer, σ the roughness, and *dens* the density in formula units (FU) per cubic angstrom. The intensity of the incident beam and the background intensity are denoted as I_0 and I_{bkg}, respectively. The quality of a fit is given as FOM log (FOM = Figure Of Merit).

	OCP	**–0.14 V**
rooflike IrO_2(110)		
d / Å	24.6	23.9
σ / Å	8.9	9.0
dens / FU·Å^{-3}	0.0182	0.0129
flat IrO_2(110)		
d / Å	48.3	50.6
σ / Å	13.3	17.3
dens / FU·Å^{-3}	0.0312	0.0312
RuO_2(110)		
d / Å	19.9	19.9
σ / Å	7.4	6.9
dens / FU·Å^{-3}	0.0311	0.0319
RuO_2 interlayer		
d / Å	2.5	2.5
σ / Å	2.0	2.0
dens / FU·Å^{-3}	0.0344	0.0331
Ru(0001) substrate		
σ / Å	54.7	56.7
inst.set		
I_0	$6.15 \cdot 10^6$	$6.92 \cdot 10^6$
I_{bkg}	1.66	1.59
FOM log	$3.05 \cdot 10^{-2}$	$2.35 \cdot 10^{-2}$

For the fitting of the XRR data the software package GenX[2] (v. 2.4.10) was utilized. A four-layer model (cf. **Figure S4**) similar to that of a previous contribution[1] was employed. Two of the layers were introduced as IrO_2 layers, the other two as RuO_2 layers. The substrate was set to metallic Ru while H_2O was employed as ambient medium. After editing the instrument parameters (wavelength, beam width/shape) and applying the fit model each imported data set was fitted manually until a rough visual agreement of the experimental data and the fit was achieved. After that the automated fitting function of GenX[2] was started and run for at least 1,000 generations. This procedure of manual and automated fitting was repeated until the experimental and fitted XRR curves were in sufficient agreement and reasonable parameters for the fit model were obtained.

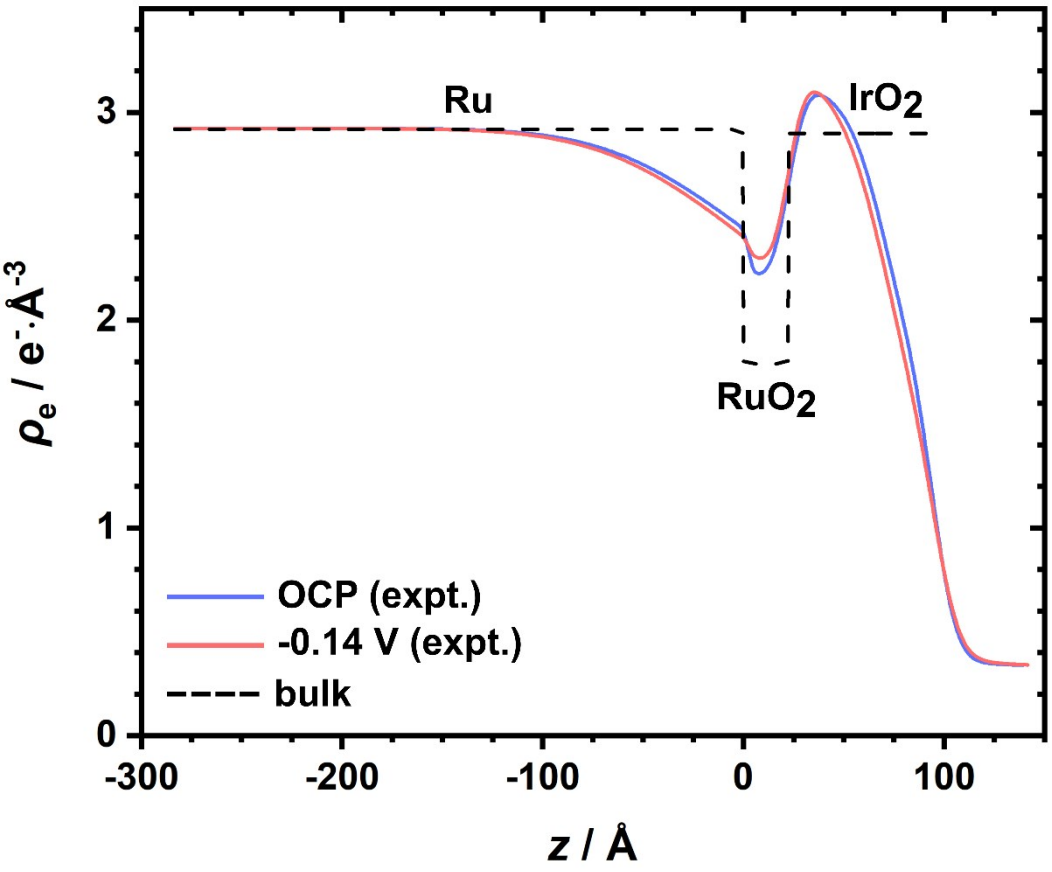

Figure S5: Experimental ("expt.") electron density profiles (solid lines) as obtained from the XRR fits at OCP and −0.14 V. For comparison, the bulk electron densities of Ru, RuO_2, and IrO_2 are shown (dashed line). *z* denotes the distance from the Ru(0001) substrate surface.

Figure S5 shows the experimental electron density profiles as derived from the fits of the XRR data at OCP (blue solid line) and −0.14 V (red solid line). For comparison, the bulk electron densities of Ru, RuO_2, and IrO_2 (black dashed line) are given. The profiles illustrate the layered structure of the model electrode. The apparently large discrepancy between the expected bulk and fitted densities for RuO2 and IrO2 in **Figure S5** is partly due to the way the plot is generated from the fitted densities, thicknesses and roughness for each slab in the model.

Table S2: Fitting parameters (CasaXPS, v. 2.3.18) of the XPS data (Ir 4f and O 1s) of the IrO_2(110)-RuO_2(110)/Ru(0001) model electrode before and after the in situ experiments. The functions for the Line Shapes are adapted from literature[3,4] and the obtained binding energies can be compared with literature[3,5,6].

freshly prepared			
component	**BE / eV**	**FWHM**	**Line Shape**
		Ir 4f	
Ir^{IV} $4f_{7/2}$	61.7	1.4	LF(0.3, 1.2, 55, 200)
Ir^{IV} $4f_{5/2}$	64.7	1.4	LF(0.3, 1.2, 55, 200)
Ir^{IV} $5p_{1/2}$	64.7	4.5	GL(30)
		O 1s	
O^{II-}	530.0	1.3	LF(0.37, 1.2, 25, 110)
after in situ experiments			
component	**BE / eV**	**FWHM**	**Line Shape**
		Ir 4f	
Ir^{IV} $4f_{7/2}$	61.7	1.3	LF(0.3, 1.2, 55, 200)
Ir^{IV} $4f_{5/2}$	64.7	1.4	LF(0.3, 1.2, 55, 200)
Ir^{IV} $5p_{1/2}$	64.7	4.5	GL(30)
		O 1s	
O^{II-}	530.0	1.4	LF(0.37, 1.2, 25, 110)
OH	531.6	2.9	GL(10)

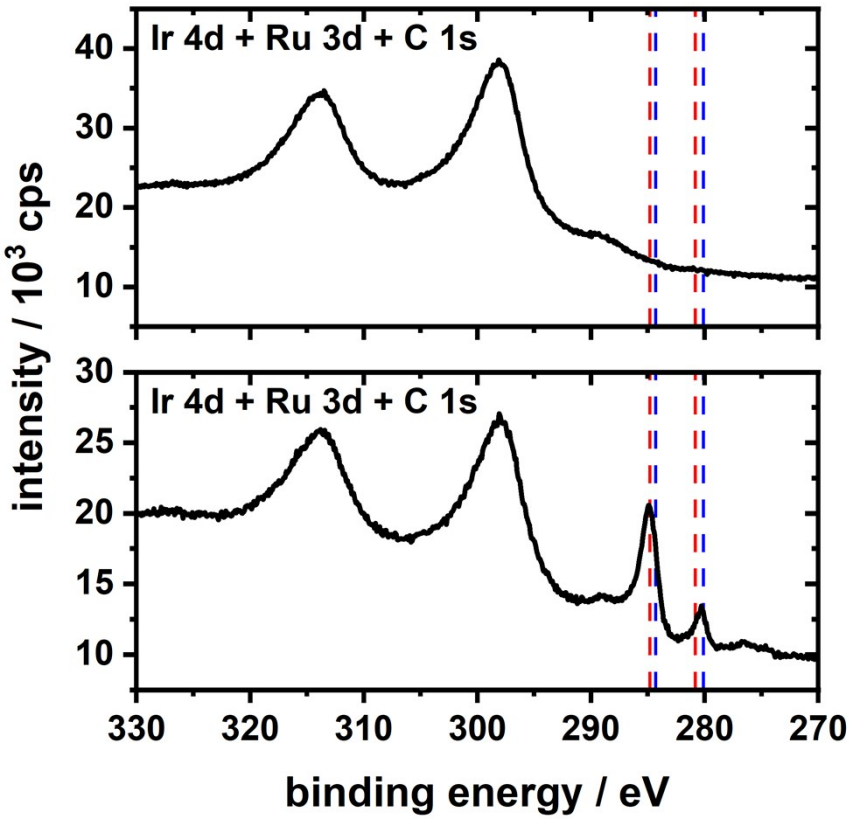

Figure S6: XP spectra in the binding energy region of Ir 4d, Ru 3d, and C 1s of the IrO_2(110)-RuO_2(110)/Ru(0001) model electrode before (top) and after (bottom) the in situ experiments. The positions of the Ru 3d signals of Ru(0001) and RuO_2(110) are indicated by dashed blue and red lines, respectively.

The XP spectrum of the freshly prepared model electrode (cf. top of **Figure S6**) reveals two peaks at binding energies of 298.1 eV and 314.0 eV, corresponding to the Ir $4d_{5/2}$ and Ir $4d_{3/2}$ signal, respectively.[3] The dashed blue and red lines indicate the positions of the Ru 3d signals corresponding to Ru(0001) and RuO_2(110), respectively.[4,7] Since the C 1s signal is overlapping with the Ru $3d_{3/2}$ peak, the intensity ratio due to spin orbit splitting of the Ru 3d signal is not preserved.

1 T. Weber, J. Pfrommer, M. J. S. Abb, B. Herd, O. Khalid, M. Rohnke, P. H. Lakner, J. Evertsson, S. Volkov, F. Bertram, R. Znaiguia, F. Carlà, V. Vonk, E. Lundgren, A. Stierle, H. Over, *ACS Catal.*, 2019, **9**, 6530-6539.

2 M. Björck, G. Andersson, *J. Appl. Cryst.*, 2007, **40**, 1174-1178.

3 S. J. Freakley, J. Ruiz-Esquius, D. J. Morgan, *Surf. Interface Anal.*, 2017, **49**, 794-799.

4 T. Weber, M. J. S. Abb, O. Khalid, J. Pfrommer, F. Carlà, R. Znaiguia, V. Vonk, A. Stierle, H. Over, *J. Phys. Chem. C*, 2019, **123**, 3979-3987.

5 V. Pfeifer, T. E. Jones, J. J. Velasco Vélez, C. Massué, R. Arrigo, D. Teschner, F. Girgsdies, M. Scherzer, M. T. Greiner, J. Allan, M. Hashagen, G. Weinberg, S. Piccinin, M. Hävecker, A. Knop-Gericke, R. Schlögl, *Surf. Interface Anal.*, 2016, **48**, 261-273.

6 M. J. S. Abb, B. Herd, H. Over, *J. Phys. Chem. C*, 2018, **122**, 14725-14732.

7 H. Over, *Chem. Rev.*, 2012, **112**, 3356-3426.